Unidirectional focusing of horizontally polarized shear elastic waves electromagnetic acoustic transducers for plate inspection

S.L. Huang[1], H. Y Sun[1], Q. Wang[2], S. Wang[1], and W. Zhao[1]

1. Department of Electrical Engineering, Tsinghua University, 100084 Beijing, P. R. China.
2. Department of Engineering, Durham University, Durham, DH1 3LE, United Kingdom

The ultrasonic guided wave testing method is very effective in monitoring the safety of complex structures. The fundamental shear horizontal (SH) wave mode has the advantage that the propagation velocity does not change with the frequency. However, accurately recognizing the ultrasonic signal is difficult due to the SH guided wave's bidirectional propagation characteristics generated by the Lorentz force mechanism. Therefore, it is necessary to achieve unidirectional focusing of Lorentz force-generated SH guided waves. A newly designed SH guided wave electromagnetic acoustic transducer (EMAT) is proposed with an interlaced periodic permanent magnet (PPM) and AC coils of different phases. A 3D model based on the electromagnetic mode and the solid mechanics mode using COMSOL software is calculated and compared with the bidirectional focusing EMATs. The results show that there are many influencing factors in the structural design of the transducers, and the focal radius and the angle of the individual PPMs are discussed in this work. The results indicate that the new unidirectional EMAT shows superiority in many cases, and the decrease of the focal radius with a suitable aperture angle will increase the focusing intensity of the signal.

1 Introduction

During the reflection, interface or waveform conversion of an ultrasonic body wave constrained by the physical boundary of a specimen such as a steel plate and pipe, an ultrasonic guided wave can form and propagate along the specimen[1-3]. The ultrasonic guided wave detection technology using a traditional piezoelectric ultrasonic transducer is commonly used for on-line detection of steel plates[4]. Piezoelectric ultrasonic transducers require a couplant to introduce ultrasonic vibrations into the specimen; therefore, application of the piezoelectric transducer is limited by conditions such as the temperature and pressure. It is because the couplant is always sensitive to variations in such factors[5-7]. Electromagnetic acoustic transducers (EMAT) mainly replace the need for a couplant as they use electromagnetic acoustic coupling and offer the advantages of easy adjustment of the equipment and wide application[8-11]. However, the low energy conversion efficiency of systems involving EMAT has always been a major challenge in non-destructive testing (NDT).

Non-dispersive fundamental shear horizontal (SH0) waves are of practical importance in guided wave inspection as changes in the frequency does not affect the propagation velocity of shear horizontal (SH) guided waves in the SH0 mode[12-14]. Due to the symmetrical structure of the transducer, SH guided waves generally propagate in both directions along the excitation direction of the ultrasonic waves on the specimen surface [15-16]. When taking measurements, attention is usually paid to whether there is a defect in a specific direction or a point in general. A wave propagating along the unfocused side only makes it difficult to identify the signal of the guided waves and extract them from the noise. Therefore, it is necessary to focus the guided wave signal on the focused side and suppress the signal on the unfocused side. In 1990, using the method of structural interference, Thompson developed the periodic permanent magnet (PPM) EMAT, which can be used to excite unidirectional SH guided waves and apply current pulses of different excitation frequencies to achieve angular control of the SH guided wave emission[17]. However, in method, the intensity of the signal obtained can weaken on using the wideband signal utilized to change the emission angle and lead to small defects not being detected. In 2016, a novel direction-controllable SH wave EMAT was proposed by Zhang et al. based on the principle of magnetostriction in a steel plate[18]. A mechanical structure that can be rotated with directional selectivity of the coils was proposed by Zhang to control the direction in which the SH guided wave is excited. However, although the structure of the EMAT can only select the propagation direction of the SH wave, it does not improve the signal strength of the SH guided wave. In 2017, Song et al. focused the beam on one side by using two EMAT coils and rotating the traditional parallel coils by an angle[19]. However, the number of transducers and the size can bring significant limitations on the application of this kind of transducers. In summary of the above findings, our work aims to improve the efficiency of the transducer as much as possible without destroying its inherent advantages. In previous studies, we proposed a newly designed fan-shaped PPM focusing coils EMAT (FPFC-EMAT) wherein the focusing characteristic of the new transducer proved to be very effective in simulations and experimental verification. A new unidirectional point-focusing SH-wave EMAT is developed in this study based on our previous research, which optimizes the focusing effect of the EMAT.

This work proposes a newly designed unidirectional point-focusing SH wave EMAT with an interlaced PPM, wherein a new transducer structure is designed and discussed in detail. The transducers studied recently were compared to the unidirectional transducers used in this study. The simulation results of the displacement field distributions for the

bidirectional and unidirectional focusing EMAT at 10 μs are provided. The effects of the focal radius and aperture angle of the individual coil on the unidirectional focusing EMAT are also investigated. The results show that the newly proposed SH guided wave EMAT performs well with respect to the unidirectional focusing effect of the signal.

2 Model description

The SH guided wave is mainly generated by two mechanisms as follows: One based on the magnetostriction principle and one based on the Lorentz force principle to excite the SH guided wave. In the detection of nonferromagnetic materials such as an aluminum plate, SH guided waves are mostly generated by the Lorentz force mechanism. Such transducers typically require a parallel alternating current (AC) coil to create a dynamic varying magnetic field that can create eddy currents on the surface of the aluminum plate. Meanwhile, PPMs along the normal direction of the plate surface are required to provide a staggered varying bias magnetic field. Due to the low energy conversion efficiency of the EMAT, the SH guided waves are also relatively unfocused, so designing a new transducer structure that can focus the guided wave signal is necessary.

This study proposes a new transducer structure that enhances the intensity of the signal on the focusing side and weakens the signal intensity on the other side, thereby improving the direction sensitivity, resolution, and signal-to-noise ratio. Figure 1(a) shows the schematic diagram of the new transducer with interlaced period permanent magnets and AC coils of different phases. We can see from the figure that the arrangement of the transducers is not strictly interlaced but is symmetrically distributed along the x-axis of the aluminum plate's center.

(a)

(b)
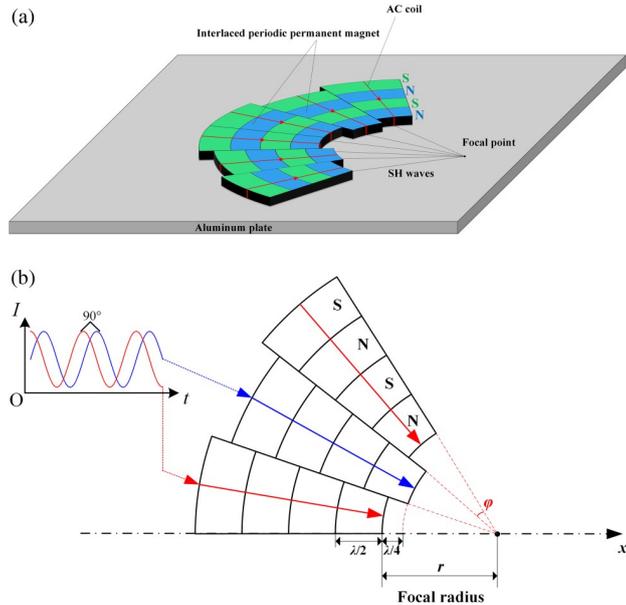
Figure 1: Schematic diagram of the newly designed unidirectional SH guided wave focusing electromagnetic

ultrasonic transducer: (a) Configuration of the new EMAT structure. (b) Two-dimensional schematic setup.

The purpose of designing the particular structure of the new transducer is to focus the signal at focal point to improve the focusing intensity and signal resolution. Since the propagation direction of the SH guided wave can be determined and the guided wave of the SH0 mode has no dispersion phenomenon, the focus of the guided wave can be achieved by arranging the coils' positions appropriately. We can see that all of the coils are concentric with interlaced PPMs, so the center is the position of the predetermined focal point. The transducer's design utilizes interlaced PPMs and two AC coils with a 90° phase difference. To achieve the unidirectional superposition propagation of the signal while suppressing the SH guided wave on the other side, the phase shift of the alternating current and the distance between the positions of the two SH wave radiation points must meet the following requirements:

$$ x_i - x_{i+1} = \frac{c_s}{4f} = \frac{\lambda}{4} \tag{1} $$

where x_i and x_{i+1} are the distances from the adjacent radiation points to the focal point, c_s is the velocity of the shear waves, f is the frequency, and λ is the wavelength.

To describe the structure of the transducer, Fig. 1(b) is a schematic diagram of the geometry. Note that the phase shift between the excitation currents of adjacent coils is 90°, so the SH wave can propagate in one direction and focus on one point using the above method. The spacing of the interlaced PPMs is $\lambda/2$, and the difference in the focus radius r between two adjacent permanent magnets is $\lambda/4$ in the transducers. The focal radius refers to the distance from the focused side of the coil to the focal center and ψ is the aperture angle of the individual PPM.

The Maxwell equations are utilized to describe the electromagnetic transformation process of the simulation model.

$$ \nabla \times \boldsymbol{H} = \boldsymbol{J}, \tag{2} $$

$$ \nabla \times \boldsymbol{E} = -\frac{\partial \boldsymbol{B}}{\partial t}, \tag{3} $$

where H is the magnetic field; J is the current density; E is the electric field; B is the magnetic flux density. Also, Gauss's law for the electric field and magnetic field should be satisfied as follows.

$$ \nabla \cdot \boldsymbol{D} = \rho, \tag{4} $$

$$ \nabla \cdot \boldsymbol{B} = 0, \tag{5} $$

where ρ is the charge density. Two constitutive equations are

utilized to solve the equations above:

$$D = \varepsilon E \qquad (6)$$

$$B = \mu H \qquad (7)$$

where ε is the dielectric constant and μ is the magnetic permeability.

Eddy current mainly exists in the skin depth of the specimen's surface, and a periodic Lorentz force is generated to excite the ultrasonic wave with the bias magnetic field.

The dynamic magnetic field equation of the pulse eddy current is

$$\frac{1}{\mu}\nabla^2 A - \sigma\frac{\partial A}{\partial t} + \frac{1}{S}\iint_s \sigma\frac{\partial A}{\partial t}\,ds = -\frac{i}{S}, \qquad (8)$$

where A is the magnetic vector potential; σ is the conductivity of the material; i is the total current; S is the cross-sectional area of the coil conductor. The induced eddy current density is

$$J_e = -\sigma\frac{\partial A}{\partial t}. \qquad (9)$$

Also, the Lorentz force F_v will increase with the increase of the eddy current density.

$$F_v = J_e \times (B_d + B_s), \qquad (10)$$

where B_d is the dynamic flux density; B_s is the static flux density of the permanent magnet. Lorentz force, as a coupling factor connecting the two models, plays an important role in the simulation.

The wave equation shown equals to the Navier's equation in the isotropic elastic solid medium is

$$(\lambda' + \mu')\nabla\nabla \cdot u + \mu'\nabla^2 u + F_v = \rho\frac{\partial^2 u}{\partial t^2}, \qquad (11)$$

where u is the displacement vector; t the time; ρ the density; F_v the volume force vector which can be obtained from the calculation of the Lorenz force in the electromagnetic field model; λ' and μ' are the Lame's constants of the material.
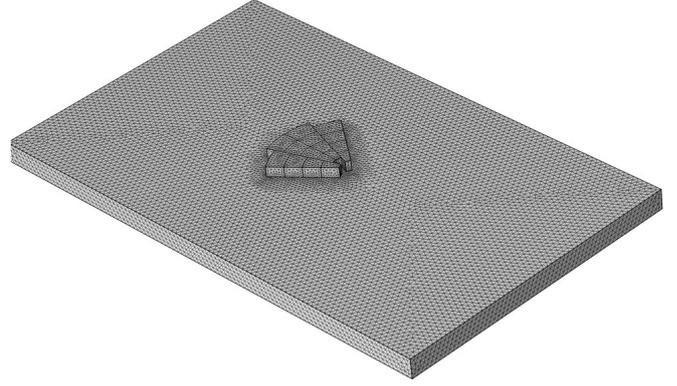
Figure 2: Meshing of simulation domain including the PPM, coils, and aluminum plate (the air domain is omitted).

A three-dimensional model of the SH guided wave focusing electromagnetic acoustic transducer has been established by using the Finite Element Method (FEM) of COMSOL numerical simulation software. The calculation domain includes air, aluminum plates, coils, and PPMs. The electromagnetic field model is calculated throughout the calculation domain, while the elastic dynamic model is only applied on the aluminum plate. The two physical fields are unidirectionally coupled by their respective physical quantities. For example, the current density calculated by the electromagnetic field can be used as the Lorentz force current source of the solid mechanical field. When meshing the solution area, in order to ensure the accuracy of the eddy current calculation, at least seven grids should be ensured to be divided in the skin depth. Also, to ensure the accurate calculation of the ultrasonic SH waves, there should be at least seven grids in one wavelength. Therefore, to satisfy the above requirements, the meshing in the calculation domain is shown in Fig. 2 where the air domain is omitted in the figure. The meshing parameters are shown in Table I while other parameters of the model are shown in Table II.

TABLE I. Unit dimension parameter of mesh generation.

Number of elements	Average element quality	Unit volume ratio
2 569 354	0.971	1.223×10^{-4}

TABLE II. Parameters of the SH guided wave EMAT.

Parameters	Value
Lift-off distance (mm)	1
Lame's constants λ' (GPa)	58
Lame's constants μ' (GPa)	29
Aluminum specimen mass density (kg/m³)	2 832
Aluminum specimen conductivity (S/m)	3.65×10^7
Remanent magnetism of the magnet (T)	1.2
Relative permeability of the magnet	400

In the calculation, the size of the aluminum plate is 200 × 100 × 1 mm³. In order to avoid excessive simulation time and improve efficiency, the PPM is divided into four parts and is arranged symmetrically. According to the propagation

velocity of the SH guided waves (c_s= 3.2 km/s) and the geometrical dimensions of the aluminum plate and avoiding the reflection, the calculation time should be less than 15 μs. Therefore, the displacement field distribution at the simulation time of 10 μs is selected and shown in the study.

3 Results and Discussion

A. Simulation Results

To investigate the characteristics of a unidirectional SH guided wave focusing EMAT, a focusing transducer that has been studied previously is utilized to compare the differences between the two transducers. Figure 3 shows the configuration of the bidirectional focusing EMAT, while the other parameters remain unchanged. The difference between the two models is that the PPMs of the unidirectional focusing SH wave EMAT differ in position and interlaced arrangement, so the coils' positions are also different. The difference in the current phase between adjacent coils is 90°, and the radial distance difference between adjacent PPMs is a quarter wavelength of 0.8 mm. The coil's AC frequency is 1 MHz and the predetermined focal radius is 20 mm.

When the simulation time reaches 6.25 μs, the SH guided wave will reach its focal point, so the simulation time is selected as 10 μs. The magnitude of the total displacement vector is shown for the bidirectional focusing EMAT [Fig. 4(a)] and the unidirectional focusing EMAT [Fig. 4(b)] at 10 μs. Figure 4 shows that although the improvement in signal intensity on the focused side is not significant, the amplitude of the displacement on the divergent side of the unidirectional focusing EMAT is suppressed on the unfocused side. To analyze the results of the unidirectional focusing quantitatively, the distributions of the displacement field for the two EMATs along the x-axis direction of the aluminum plate surface centered at 10 μs are shown in Figs. 5(a) and 5(b). Figure 5(a) shows that the displacement at the focal point is 2.46 × 10−12mm while the displacement that corresponds to the focusing position on the other side is 1.4 × 10−12mm. Regarding the unidirectional focusing EMAT shown in Fig. 5(b), the displacement is 2.55 × 10−12mm at the focal point and 0.82 × 10−13mm on the other side. Comparing the simulation results shows that the use of a unidirectional focusing EMAT significantly weakens the intensity of the signal on the unfocused side. The amplitude of the displacement on the unfocused position is reduced to 63.6% of the original signal intensity while the displacement amplitude of the focal point position also improves by 3.7% using the new unidirectional focusing EMAT.
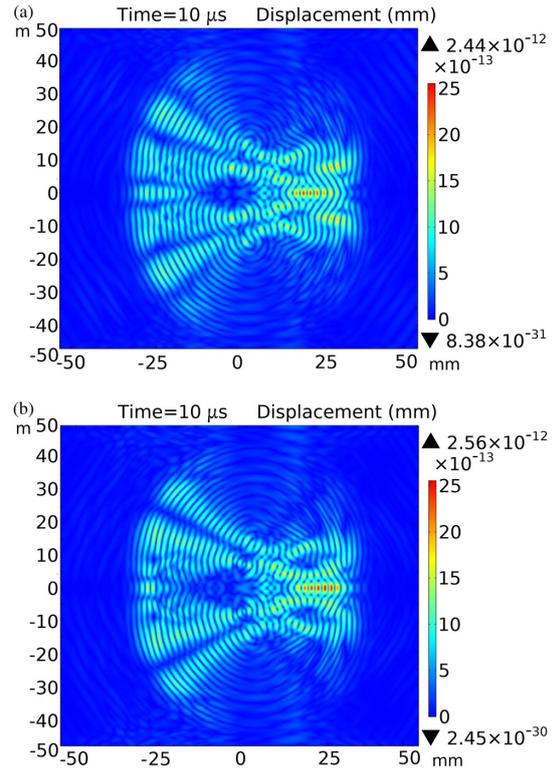
Figure 4: Simulation results for the focusing EMAT and the distribution of the displacement field on the aluminum plate at 10 μs: (a) Bidirectional focusing EMAT; (b) unidirectional focusing EMAT.

B. Experimental configuration

The experiment configuration shown in Fig. 6 has been built to verify the influence of the focal radius on the performance of the newly designed EMAT. In the detection, we utilized the newly designed unidirectional focusing EMAT to excite and receive ultrasonic signals. Unlike the excitation processes of other waves, the excitation of the SH wave based on the Lorentz force requires the support of tightly wound coils, which is unsuitable for the precise control of the printed coils on a printed circuit board (PCB), so it is necessary to determine a reasonable arrangement for the coils. Pulsed power (RPR 4000) for generating and receiving signals are utilized in the experimental research. The power both produces strong and stable sinusoidal high-frequency pulses and identifies and receives the desired signals over a broad frequency band. An oscilloscope (TDS 1002) is utilized to display the waveform acquired by the RPR-4000, which has a 60MHz bandwidth and 1 Gs/s sampling rate. Impedance matching is achieved by connecting a 150-Ω resistor in parallel with the coil. In the excitation signal, the bandwidth is 4MHz and the central frequency is 1MHz.
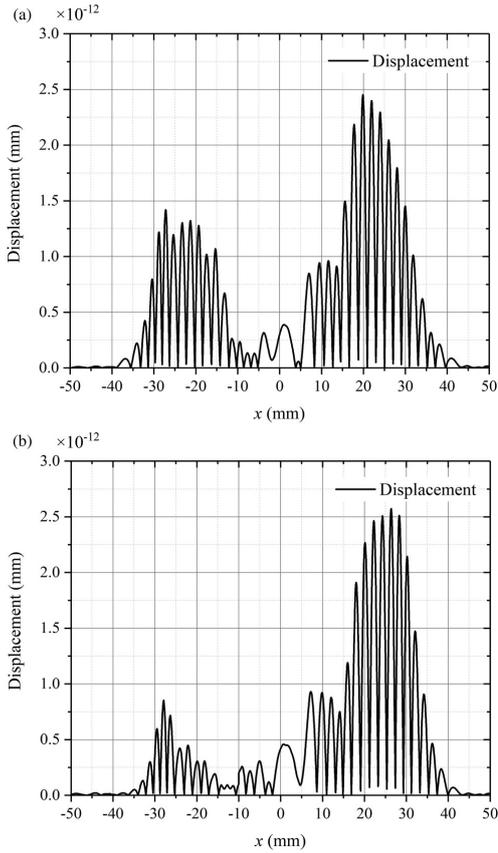
Figure 5: Simulation results for the focusing EMAT and the displacement distribution along the x-axis on the aluminum plate at 10 μs: (a) Bidirectional focusing EMAT; (b) unilateral focusing EMAT.

Figure 6: Experimental configuration for the focusing coils EMAT.

Regarding the total displacement vector on the focused and unfocused sides, we experimented with the same conditions and measured the displacement on the unfocused side of the corresponding focusing position. In this work, the x-direction is the SH guided wave propagation direction, and the y-direction is the vibration direction. Moreover, we compared the experimental and simulation results on the focused and unfocused sides. For comparison purposes, we normalized the results but retained the negative values. Figure 7(a) shows the simulation and experiment results on the unfocused side, and Fig. 7(b) shows the results on the focused side. We note that the normalized signal amplitude on the unfocused side of the simulation was 0.29; this was 0.32 in the experiment. For the focused side, it was 0.91 in the simulation and 1 in the experiment.

It is worth noting that there are discrepancies between the simulation and the experimental signals, particularly on the right side of the signal (Fig. 7). In the experiment, the errors of the excitation power, transducer position, and waveform asymmetry caused by the material and geometry of the specimen will reduce the accuracy of the experimental results. However, in the ultrasonic guided wave detection, the amplitude of signals and time of flight (TOF) should be considered two critical parameters in the measurement. Therefore, the experimental results are in reasonable agreement with the simulation results in this work.

C. Effects of the focal radius and the aperture angle

The wave has attenuated during the propagation process, so the selection of the focusing position is significant. To analyze the influence of the focal radius on the amplitude of the displacement at the focal point, five different focal radii such as 10, 15, 20, 25, and 30mm are simulated and verified by the experiment. The simulation parameters are consistent with those utilized in the experiment, and the lengths of the focal radius can be varied by designing the structure of the transducers. Figure 8 shows the simulation results and the experiment results at different focal radii, and the normalized displacements at the focal point are also shown in this figure.

(a)

(b)
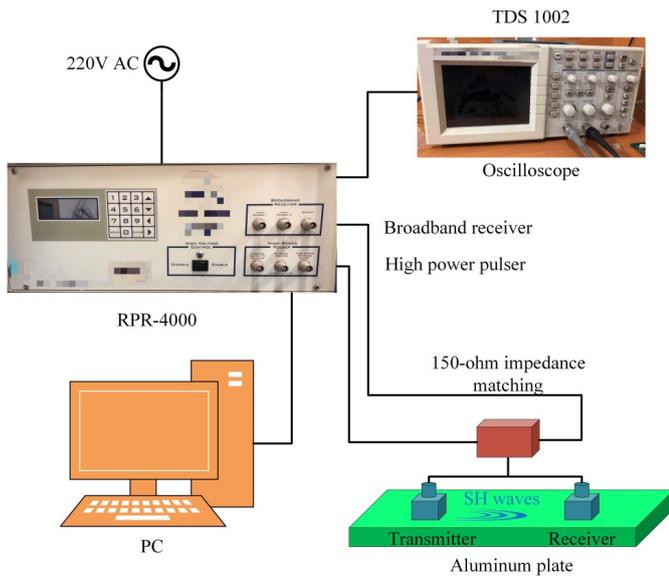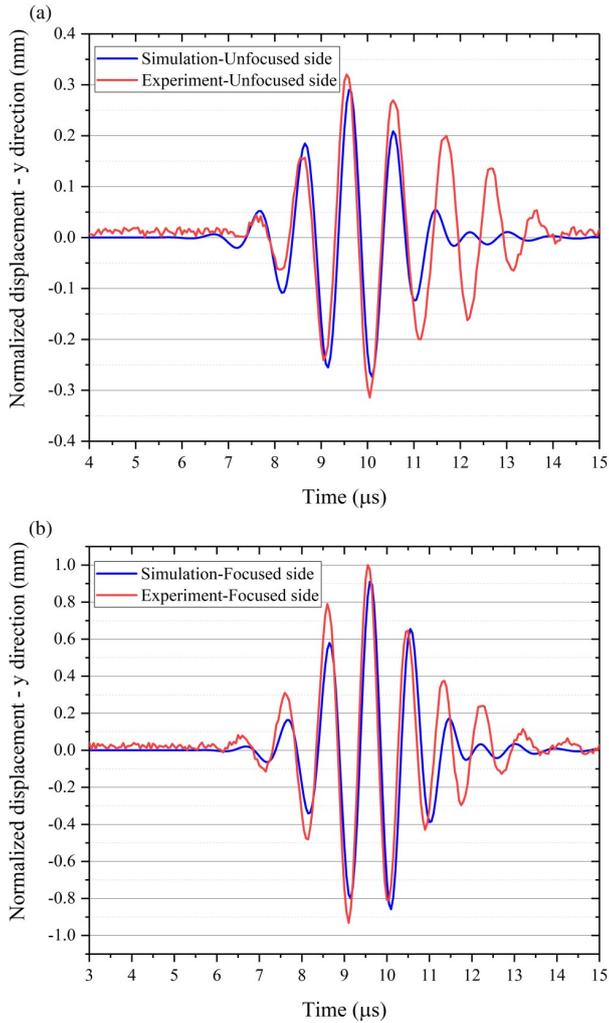
Figure 7: Simulation and experiment results on (a) the unfocused side; (b) the focused side.

To make an intuitive comparison, the results have been normalized, and it can be found that the simulation results are in good agreement with the experimental results. The blue line in the figure represents the simulation result, and the red line represents the experimental results. It can be seen from the figure that as the focus radius increases, the magnitude of the displacement at the focal position decreases parabolically for both simulation and experiment data. Among all the measured focal radii, the smallest focal radius (10 mm) has the largest displacement amplitude. Moreover, the signal intensity at the focusing position with 30 mm focal radius is the weakest, and the ultrasonic energy attenuation can be explained as the propagation distance increases.
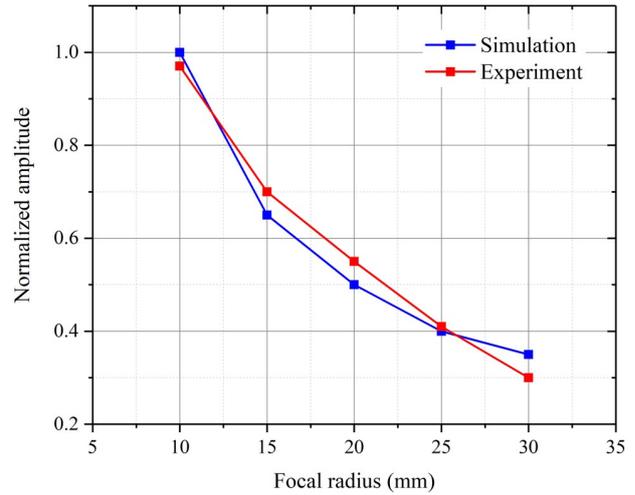
Figure 8: Simulation and experimental results: the effect of focal radius on the normalized displacement amplitude.

In the structural design of the new transducer, the structure of each PPM has a great influence on the focusing effect of the signal. While the spacing of the PPMs has been determined to be a half wavelength, the magnitude of the signal strength at the focal point can be obtained by changing the aperture angle of each PPM while the number of magnetic poles of the magnet remains unchanged. Therefore, five aperture angles such as 5°, 10°, 15°, 20°, and 25° are chosen to obtain the displacements at different aperture angles in Fig. 9, and the displacements at different angles are normalized to the maximum.
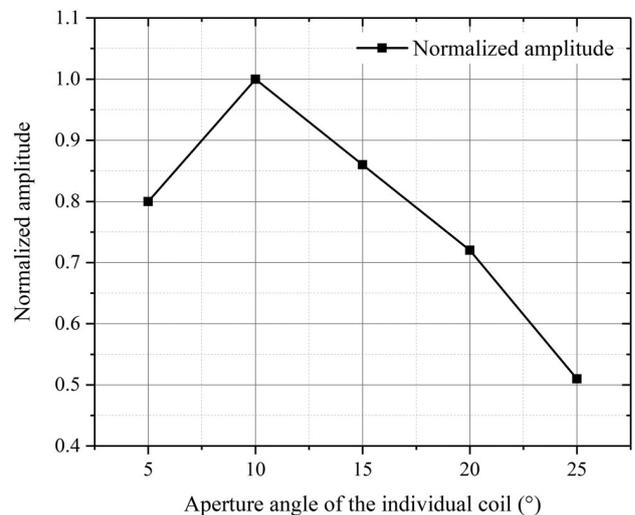
Figure 9: Normalized displacements at different aperture angles of the individual coil.

Since the total number of unidirectional permanent magnets is fixed to three, it is convenient to compare the influence of the aperture angle of the permanent magnet on the displacement at the focal point. It can be seen from the figure that the normalized amplitude of the displacement at the focal point reaches the maximum when the aperture angle is 10°

rather than the minimum value of 5°. When the aperture angle is larger than 10°, the normalized amplitude of the displacement at the focal point decreases with the increase of the aperture angle. The reason for the nonmonotonic displacement characteristic is that when the aperture angle is too small, there will be mutual interference between adjacent alternating PPMs, which causes the magnetic field close to the coil not perpendicular to the plate plane. It may cause off-plane displacement or other modes of waves on the plate, which weakens the signal intensity of the focusing position. As for the angle larger than 10°, the larger the aperture angle, the weaker the waveform superposition at the focusing position, so the displacement at the focal point is smaller.

4 Conclusion

A newly designed unidirectional focusing SH wave EMAT with an interlaced PPM is proposed in this work. A three-dimensional model including the electromagnetic mode and the elastic dynamics mode is established to calculate the propagation and focusing process of the SH guided wave. In comparison with the calculation results of the bidirectional point-focusing EMAT, the signal amplitude of the new transducer on the unfocused side is reduced to 63.6%, which is a useful improvement in terms of avoiding the signal's overlap and interference. In the structural design of the new transducer, two critical factors, the focal radius and the aperture angle, are investigated while the former is studied by numerical simulation and experiment. The results show that an increase in the focus radius leads to a decrease in the signal focus intensity. As for the effect of the aperture angle of the individual coils, both lower and higher aperture angles will weaken the signal to some extent. Therefore, the aperture angle of the transducer of the newly designed EMAT needs to be selected properly.

Acknowledgements

References

1 A. Velichko and P. D. Wilcox, "Excitation and scattering of guided waves: Relationships between solutions for plates and pipes," J. Acoust. Soc. Am. 125, 3623 (2009).

2 H. Ogi, M. Hirao, and T. Ohtani, "Line-focusing of ultrasonic SV wave by electromagnetic acoustic transducer," J. Acoust. Soc. Am. 103, 2411 (1998).

3 H. Ogi, M. Hirao, and T. Ohtani, "Line-focusing electromagnetic acoustic transducers for the detection of slit defects," IEEE Trans. Ultrason. Ferr. 46, 341 (1999).

4 P. S. Lowe, R. M. Sanderson, N. V. Boulgouris, A. G. Haig, and W. Balachandran, "Inspection of cylindrical structures using the first longitudinal guided wave mode in isolation for higher flaw sensitivity," IEEE Sens. J. 16, 706 (2016).

5 M. Hirao and H. Ogi, EMATs for Science and Industry: Noncontacting Ultrasonic Measurements (Springer, 2003).

6 P. A. Petcher and S. Dixon, "Weld defect detection using PPM EMAT generated shear horizontal ultrasound," NDT E Int. 74, 58 (2015).

7 X. Zhao and J. L. Rose, "Guided circumferential shear horizontal waves in an isotropic hollow cylinder," J. Acoust. Soc. Am. 115, 1912 (2004).

8 S. Dixon, C. Edwards, and S. B. Palmer, "Texture measurements of metal sheets using wideband electromagnetic acoustic transducers," J. Phys. D Appl. Phys. 35, 816 (2002).

9 X. Jian, I. Baillie, and S. Dixon, "Steel billet inspection using laser-EMAT system," J. Phys. D Appl. Phys. 40, 1501 (2007).

10 X. Jian, S. Dixon, I. Baillie, R. Edwards, and J. Morrison, "Integrity evaluation of steel products using EMATs," J. Phys. D Appl. Phys. 40, 300 (2007).

11 R. Edwards, S. Dixon, and X. Jian, "Enhancement of the Rayleigh wave signal at surface defects," J. Phys. D Appl. Phys. 37, 2291 (2004).

12 C. F. Vasile and R. B. Thompson, "Excitation of horizontally polarized shear elastic waves by electromagnetic transducers with periodic permanent magnets," J. Appl. Phys. 50, 2583 (1979).

13 H. Kwun and C. M. Teller, "Magnetostrictive generation and detection of longitudinal, torsional, and flexural waves in a steel rod," J. Acoust. Soc. Am. 96, 1202 (1994).

14 R. Murayama, S. Makiyama, M. Kodama, and Y. Taniguchi, "Development ofan ultrasonic inspection robot using an electromagnetic acoustic transducer for a lamb wave and an SH-plate wave," Ultrasonics 42, 825 (2004).

15 H. Ogi, E. Goda, and M. Hirao, "Increase of efficiency of magnetostriction SH-wave electromagnetic acoustic transducer by angled bias field: Piezomagnetic theory and measurement," Jpn. J. Appl. Phys. 42, 3020 (2003).

16 S. Hill and S. Dixon, "Frequency dependent directivity of periodic permanent magnet electromagnetic acoustic transducers," NDT E Int. 62, 137 (2014).

17 R. B. Thompson, "Physical principles of measurements with EMAT transducers," Phys. Acoust. 19, 157 (1990).

18 Y. Zhang, S. Huang, S. Wang, and W. Zhao, "Direction-controllable electromagnetic acoustic transducer for SH waves in steel plate based on magnetostriction," Prog. Electromagn. Res. Symp. 50, 151 (2016).

19 X. Song and G. Qiu, "Optimization of a focusable and rotatable shear-wave periodic permanent magnet electromagnetic acoustic transducers for plates inspection," Sensors 17, 2722 (2017).